



Published in final edited form as:

Nat Microbiol. ; 1(11): 16144. doi:10.1038/nmicrobiol.2016.144.

Cell-to-cell spread of microsporidia causes *Caenorhabditis elegans* organs to form syncytia

Keir M. Balla, Robert J. Luallen, Malina A. Bakowski, and Emily R. Troemel*

Division of Biological Sciences, Section of Cell and Developmental Biology, University of California, San Diego, 9500 Gilman Drive, La Jolla, CA 92093

Abstract

The growth of pathogens is dictated by their interactions with the host environment¹. Obligate intracellular pathogens undergo several cellular decisions as they progress through their life cycles inside of host cells². We studied this process for microsporidian species in the genus *Nematocida* as they grew and developed inside their co-evolved animal host *Caenorhabditis elegans*³⁻⁵. We found that microsporidia can restructure multicellular host tissues into a single contiguous multinucleate cell. In particular, we found that all three *Nematocida* species we studied were able to spread across the cells of *C. elegans* tissues before forming spores, with two species causing syncytial formation in the intestine, and one species causing syncytial formation in the muscle. We also found that the decision to switch from replication to differentiation in *N. parisii* was altered by the density of infection, suggesting that environmental cues influence the dynamics of the pathogen life cycle. These findings show how microsporidia can maximize the use of host space for growth, and that environmental cues in the host can regulate a developmental switch in the pathogen.

Intracellular pathogens are a diverse category of microbes that can utilize the space and resources of their host organisms for replication². After invasion of a single host cell, it is beneficial for intracellular pathogens to spread to other cells to maximize the use of host space for replication before exiting and spreading to new hosts. Several mechanisms have been described to aid dissemination by pathogens. For example, both bacteria and viruses have been shown to utilize host actin to move between host cells by inducing the uptake of a microbe-containing host cell protrusion into a neighboring cell, thereby avoiding contact with the extracellular space during dissemination⁶. Other pathogens avoid the extracellular space by coordinating the fusion of infected host cells with neighboring uninfected host cells to form syncytia^{7, 8}. These studies highlight growth strategies that can be used by intracellular pathogens to expand their access to host space *in vitro*, although pathogen dissemination can involve alternative mechanisms *in vivo*⁹. *In vivo* studies are particularly important for studying infection by eukaryotic pathogens, which have especially complex

Users may view, print, copy, and download text and data-mine the content in such documents, for the purposes of academic research, subject always to the full Conditions of use: http://www.nature.com/authors/editorial_policies/license.html#terms

*To whom correspondence should be addressed: etroemel@ucsd.edu, phone number: (858) 246-0708.

Author Contributions

KMB, RJL, and ERT designed experiments, KMB and RJL performed experiments and analyzed data, MAB generated the ERT147 transgenic strain, RJL and MAB contributed to the manuscript, KMB and ERT wrote the manuscript.

growth dynamics often involving various stages of differentiation that can take place in several specific host environments¹⁰.

Microsporidia are eukaryotic obligate intracellular pathogens that form a phylum of more than 1400 fungal-related species that can infect animals ranging from single-celled ciliates to humans¹¹. Little is known about the progression that a single microsporidia cell takes as it grows within a single host cell of an intact animal to complete its life cycle¹². Several species of microsporidia in the genus *Nematocida* have been isolated from wild-caught *Caenorhabditis* nematodes around the world^{3, 5, 13}. *Nematocida* species appear to have a life cycle that is similar to other microsporidian species: after spore-mediated invasion of host cells, *Nematocida* cells replicate in multinucleate structures called meronts and then differentiate into spores to exit the host cell and propagate infection^{3-5, 14}. The transparency and invariant cellular topology of *C. elegans* together with a collection of their natural microsporidian pathogens provides a powerful system for studying how microsporidia have evolved to grow in a whole-animal host¹⁵.

To characterize the *in vivo* growth dynamics of microsporidia inside an animal, we generated populations of synchronized *N. parisii* infections consisting of a single parasite cell in a single *C. elegans* intestinal cell and tracked the parasite life cycle over time. We pulse-inoculated *C. elegans* with *N. parisii* spores to obtain infected populations where most animals were either uninfected, or infected with a single microsporidian cell (Supplementary Table 1). To visualize infection, we fixed a fraction of the population at various hours post-inoculation (hpi) and stained using a fluorescence *in situ* hybridization (FISH) probe that targets the *N. parisii* small subunit rRNA. At 3 hpi, we found that *N. parisii* cells are small and irregularly shaped, with a single nucleus (Fig. 1a). *N. parisii* cells with two nuclei were not observed until 18 hpi (Fig. 1b), indicating that replication only occurs after a significant lag time post-infection. By 36 hpi *N. parisii* had grown to spread across several host intestinal cells (Fig. 1c). No spores had formed at this time, indicating that *N. parisii* was able to grow across the lateral cell boundaries of neighboring intestinal cells before differentiating into spores, which were previously thought to be the only transmissible stage of infection. New spores were first observed at 52 hpi, and by this time *N. parisii* had grown to fill a large fraction of the intestine (Fig. 1d,e). We quantified the growth in size of single microsporidia cell infections, and found that *N. parisii* grew to take up more than half the space of the entire intestine by the time new spores were formed (Fig. 1f).

The growth of single *N. parisii* cells across the host intestine indicated that the boundaries between neighboring host cells might be restructured during infection. To visualize host cell boundaries during single microsporidia cell infections, we infected transgenic animals expressing an intestinal GFP-tagged version of LET-413, a highly conserved protein that localizes to the basolateral membrane of polarized cells¹⁶. We observed deformation of intestinal cell boundaries as *N. parisii* grew laterally (Fig. 2a). Imaging live transgenic animals at this stage of infection demonstrated that *N. parisii* can appose an intact intestinal cell boundary and then grow across that boundary coincident with localized loss of lateral LET-413 (Fig. 2b-c, and Supplementary Video 1). We quantified this growth and found that by 27 hpi *N. parisii* infections had spread into one neighboring host cell on average, and by

the time of sporulation the parasite had spread into 12 of the 20 total host intestinal cells on average (Supplementary Fig. 1).

The results above indicate that *N. parisii* spreads across cell boundaries during growth, leading to the question of whether neighboring intestinal cells join together to share cytoplasmic space. To address this question, we generated transgenic animals that express the green-to-red photoconvertible fluorescent Dendra protein in the cytoplasm of their intestinal cells. After infecting these animals, we photoconverted Dendra in a single cell from green to red and then recorded the diffusion of the red signal. When Dendra was photoconverted in the uninfected cells within an infected animal that was infected elsewhere, we found that the red signal remained restricted to the cell in which it was converted (Fig. 2d, Supplementary Fig. 2), indicating that the cell boundaries were intact. In contrast, when Dendra was photoconverted in an infected cell, we found that the red signal diffused across all neighboring cells where infection was present (Figure 2e, Supplementary Fig. 2). These data show that *N. parisii* is able to spread across the boundaries of neighboring host cells, and in so doing causes intestinal cells to join together into syncytia. Thus, we show that a eukaryotic pathogen causes what appear to be abnormal cell fusion events in the host to allow for intercellular spread.

As in other animals, cell fusion is essential for normal development in *C. elegans* and is carefully regulated by specific fusogens¹⁷. The abnormal fusion of intestinal cells caused by *N. parisii* infection could result from exploitation of host fusogens. To test this possibility, we infected two *C. elegans* fusion mutants: epithelial fusion failure (*eff-1*) mutants and anchor cell fusion failure (*acf-1*) mutants. We observed *N. parisii* spreading in both mutant strains (60/60 infections analyzed per condition), demonstrating that these fusogens are not required for infection-induced intestinal cell fusion (Supplementary Fig. 3).

Next we investigated whether microsporidian infection-induced fusion of host cells is a conserved growth strategy by characterizing the growth of two other *Nematocida* species, *N. sp. 1* and *N. displodere*. Like *N. parisii*, *N. sp. 1* only invades and replicates in the intestine of *C. elegans*, while *N. displodere* invades and replicates within several tissues^{3, 5}. All three species of *Nematocida* appear to invade from the intestinal lumen, and *N. displodere* is thought to directly invade non-intestinal tissues from the lumen because it has a longer infection apparatus than *N. parisii*⁵. To determine whether these other *Nematocida* species cause host-tissue syncytia formation, we performed single-cell infections (Supplementary Table 1) and quantified pathogen spread. First we analyzed infections in the intestine, and here we found that both *N. parisii* and *N. sp. 1* always spread across several host intestinal cells by the time of spore formation (76 hpi), but *N. displodere* was usually restricted to a single intestinal cell by the time of spore formation (120 hpi) (Fig. 3a–c and Supplementary Fig. 4). Next, we analyzed spread in the muscle. Unlike skeletal and somatic muscle cells in other animals, the 95 body wall muscle cells of *C. elegans* do not fuse into syncytia during normal development¹⁸. However, we observed that single-cell *N. displodere* infections induced syncytia formation and grew across many host muscle cells before forming spores, while *N. parisii* and *N. sp. 1* did not invade or replicate in the muscle (0/60 animals analyzed) (Fig. 3d and Supplementary Fig. 4). Furthermore, we observed four cases of single *N. displodere* cell infections that appeared to have spread out of the large hypodermal

syncytium of *C. elegans* (*hyp7*) and into the anterior epidermal cells (Supplemental Fig. 5)¹⁹. These data demonstrate that at least among natural pathogens of nematodes, intercellular spread through host cell syncytia formation is a conserved growth strategy for microsporidia determined by species- and tissue-specific interactions.

While both *N. parisii* and *N. sp. 1* grow in the intestine of *C. elegans*, we found that single *N. sp. 1* cells spread into more host intestinal cells on average than single *N. parisii* cells by the time of spore formation (Supplementary Fig. 4). This observation indicated that there could be differences in the growth dynamics between species. To compare the dynamics of intestinal pathogen growth between species of microsporidia, we infected animals with single *N. parisii* or *N. sp. 1* cells and measured their growth rates and spore formation over time. Infections by both species grew from a single nucleated cell within an animal to approximately 50,000 nuclei during the life cycle (Fig. 4a). Interestingly, *N. sp. 1* grew slightly faster and formed spores much earlier than *N. parisii*. The average doubling times during the exponential stages of growth (18 hpi – 48 hpi) for *N. parisii* and *N. sp. 1* were 2.4 h and 2.1 h, respectively. In addition to completing its lifecycle more rapidly, *N. sp. 1* infection had a much stronger negative effect on host fitness than *N. parisii* infection. Single *N. parisii* cell infections only slightly reduced the host growth compared to uninfected animals, while single *N. sp. 1* cell infections drastically reduced host growth (Fig. 4b). Furthermore, *N. parisii* infection decreased host egg production at 60 hpi compared to uninfected animals while *N. sp. 1* infection essentially eliminated host egg production (Fig. 4c). These observations reveal that related microsporidia species can have distinct growth dynamics in the same niche and can differentially exploit host space with varied effects on host fitness.

We noticed that infection by *N. sp. 1* caused animals to be smaller than infection by *N. parisii* (Fig. 4b), and hypothesized that differences in host size might influence the timing of the decision to form new spores. To test this possibility, we infected body size mutants with single *N. parisii* cells and compared spore formation timing to wild-type animals. The *sma-6* and *lon-1* mutations occur in members of the transforming growth factor beta signaling pathway that lead to shorter or longer animals, respectively^{20, 21}. Despite the greater length of *lon-1* animals, we found that both the *sma-6* and the *lon-1* mutant strains were smaller in total area than wild-type animals (Fig. 4d). Interestingly, we found that single pathogen cell infections in these small mutant animals had formed spores earlier than wild-type animals (Fig. 4e). These differences could result from a decrease in the time it takes for *N. parisii* to fill the host intestine, potentially providing a density-dependent cue to transition into the spore formation stage. We tested for the influence of infection density on the timing of spore formation by increasing the initial number of infections per animal, which would increase the rate at which *N. parisii* fills the host tissue. Consistent with our hypothesis, we found that more spores formed when the initial number of infections per animal was increased (Fig. 4f). Importantly, we found that the growth rate of *N. parisii* was similar in hosts of different sizes and with differing numbers of initial infections, demonstrating that infection density affects the timing of spore differentiation, but does not affect the lag phase or rate of replication (Supplementary Fig. 6). Thus, host size and infection density appear to influence the timing of a switch from replication to differentiation into spores for microsporidia.

In this paper, we followed the progression of synchronized infections initiated by a single microsporidia cell in a single host cell of an intact animal from invasion until the final stage of the life cycle. The most surprising observation that we made is that *Nematocida* species spread between host cells by fusing them together into syncytia, with species- and tissue-specific patterns. It remains possible that either host- and/or pathogen-encoded fusogens mediate true cell-cell fusion, or alternatively *Nematocida* may spread to span several neighboring *C. elegans* cells by breaking down their lateral membranes instead of fusing the two lipid bilayers. Previous studies have shown that the intestinal cell integrity of *C. elegans* is maintained even at later stages of infection, indicating that cell-to-cell spread of *N. parisii* does not compromise the overall integrity of the intestinal organ^{22, 23}. Further studies on the molecular and structural changes involved in the *Nematocida-C. elegans* interactions we described here will contribute to our understanding of how two separate cells can be joined together. Previous studies on infections of both vertebrates and invertebrates reported that microsporidia cause the formation of syncytia in host tissues^{24–26}. These syncytia can occur in structures called xenomas, which are described as hypertrophic host cells that increase in size and number of nuclei²⁷. Some microsporidia-induced syncytia may therefore result from nuclear replication without host cell division rather than through fusion of neighboring host cells, but together with the evidence we present here it appears that induction of host cell fusion is a widely shared strategy for intercellular spread among diverse species of microsporidia.

Our experiments lead us to speculate that the cue for transitioning from replication to spore formation in microsporidia may be related to the sensing of host resource availability and/or the sensing of self, both of which are related to the density of infection. There is precedent for eukaryotic organisms making developmental decisions based on density, which is exemplified by several fungal species that undergo developmental switches in response to high density and nutrient availability²⁸. As has been shown for many other developmental switches in pathogens²⁹, the specific factors that regulate transitions in the microsporidia life cycle likely involve responses made by both host and pathogen to changes in their shared metabolic pool. Our finding that microsporidia can grow across a substantial portion of the cells comprising an entire animal organ before differentiating opens up a new set of questions regarding the dynamic inputs that intracellular pathogens interpret from the host environment to optimize growth and transmission.

Materials and methods

C. elegans and *Nematocida* strains

C. elegans strains were maintained on nematode growth media (NGM) seeded with *E. coli* OP50-1 (which is a streptomycin-resistant OP50 strain) as previously described³⁰. For simplicity, this strain is referred to as OP50 throughout. To obtain starved and synchronized L1 larvae, gravid adults were bleached to isolate eggs, which then were allowed to hatch overnight at 20°C³¹. The *C. elegans* wild-type N2, small mutant CB1482 *sma-6(e1482)*, long mutant CB185 *lon-1(e185)*, and intestinal GFP transgenic SJ4144 *zcIs18 [ges-1p::GFP(cyt)]* strains were obtained from the *Caenorhabditis* Genetics Center. ERT351 was derived from SJ4144 by backcrossing to N2 eight times. Transgenic animals with

intestinal expression of GFP-labeled LET-413 were generated by injection of pET213 [*vha-6p::GFP::let-413*] and a *myo-2::mCherry* co-injection marker to generate a multi-copy array strain. This strain was treated with UV psoralen at 700 μ J to generate the integrated ERT147 *kyIs21[vha-6p::GFP::let-413, myo-2::mCherry]* strain. A cytoplasmic intestinal photoconvertible fluorescent protein construct pET207 was generated using three-part Gateway recombination by fusing the intestinal-specific *vha-6* promoter to Dendra³² with the *unc-54* 3' UTR. This construct was injected into N2 animals and transgenic progeny were recovered to generate a multi-copy array strain ERT113 *kyEx46[vha-6p::dendra::unc-54 3' UTR]*. Infection experiments were performed with *Nematocida parisii* strain ERTm1, *Nematocida* sp. 1 strain ERTm2, and *Nematocida displodere* strain JUm2807³⁻⁵. Spores were prepared and quantified as previously described²².

Single microsporidia cell infections

Synchronized first-larval stage (L1) animals were inoculated with OP50 and a series of spore dilutions on NGM plates at 20°C. These animals were collected two and a half hours after plating, washed three times with PBS containing 0.1% Tween 20 to remove spores, and re-plated with OP50 at 20°C. A fraction of the population was fixed at this time with 4% paraformaldehyde (PFA) for 30 minutes, then stained by FISH with the *Nematocida* ribosomal RNA-specific MicroB probe³ conjugated to a red Cal Fluor 610 dye (Biosearch Technologies). The number of infectious events per animal was quantified in 50 animals per dosage after mounting samples on agarose pads with VECTASHIELD mounting medium containing DAPI (Vector Labs) and imaging using a Zeiss AxioImager M1 upright fluorescent microscope with a 40X oil immersion objective. A limiting dilution of *Nematocida* spores was tested to identify a concentration in which more than 83% of infected animals contained only a single microsporidia cell. The spore dosage that had this characteristic typically yielded a Poisson distribution of infection, in which an average of 72% of the population was uninfected and 28% infected. Infection distributions were measured for all experiments to ensure that the vast majority of infected animals contained a single microsporidia cell (see Supplementary Table 1).

Measuring microsporidia growth by microscopy

The ERT351 strain was infected at the L1 stage at a dosage following the parameters described above for single microsporidia cell infections. Animals were fixed at various times post-inoculation in 4% PFA for FISH staining and microscopy-based analysis of growth. Samples were mounted on 5% agarose pads and imaged using a 40X oil immersion objective or a 10X objective on a Zeiss LSM700 confocal microscope run by ZEN2010 software. Z-stacks were acquired of the entire intestinal space with a z-spacing of 1 μ m (at 400X) or 6 μ m (100X), collecting GFP signal (expressed in cytoplasm of intestine) and RFP signal (microsporidia signal stained by FISH). Analysis of these images was performed with Fiji software³³. Briefly, the brightest slice was used to threshold GFP and RFP to binary signals. The 3D objects counter function was used to measure voxels after converting signals, which were used to quantify the volume of intestine (GFP) and pathogen (RFP) in 10 animals per time point. The percentage of intestinal volume taken up by pathogen was calculated by dividing RFP voxels by the sum of RFP and GFP voxels.

Analysis of microsporidia growth across host intestinal cells

ERT147 animals were infected with a single microsporidia cell. These animals were imaged at various times post-inoculation either after being fixed and stained as described above or as live animals using a 40X oil immersion objective on a Zeiss LSM700 confocal microscope run by ZEN2010 software. For live imaging, infected ERT147 animals were mounted on 5% agarose pads with microsphere beads and imaged with a 63X oil-immersion objective for 120 cycles at 1.58 μ s pixel dwell time for five minutes. GFP was excited with a 488nm laser at 2.1% power, and light was collected with the pinhole set to 44 μ m. Quantifying growth of microsporidia across intestinal cell boundaries was performed after fixing ERT147 animals and staining by FISH as described above. To measure the diffusion of cytoplasm in intestinal cells, ERT113 animals were infected at the L1 stage and imaged live 48 hours post-inoculation with a 40X oil-immersion objective. A 488 nm laser at 0.5% power was used to excite green Dendra proteins and a 555 nm laser at 14% power was used to excite red Dendra proteins. Light was collected with a pinhole size of 42 μ m and a 3.15 μ s pixel dwell time. Dendra proteins were converted in a 4 μ m diameter space with a 405 nm laser at 35% power with a pixel dwell time of 50 μ s. Infected cells could be distinguished from uninfected cells based on exclusion of fluorescent signal. To quantify the diffusion of converted signal, the mean red signal was measured in a 15 μ m² area within the targeted cell or outside of the targeted cell (at a distance of greater than 30 μ m from targeted cell) before and two minutes after conversion.

Comparing *Nematocida* growth across different host tissues

Transgenic animals expressing GFP in the cytoplasm and nuclei of intestinal or muscle cells were infected with single *N. parisii*, *N. sp. 1*, or *N. displodere* cells at 15°C and fixed at the time of spore formation. These experiments were performed at the lower temperature of 15°C (compared to 20°C used in other infection experiments) to facilitate the growth of *N. displodere*. For the intestinal-GFP strain ERT413 *juSi21[spp-5p::GFP; cb-unc-119(+)] II*⁵, 1000 synchronized L1 larvae were grown at 20°C for 48 hours to the young adult stage before being inoculated with 3.7×10^5 *N. parisii* spores, 3.2×10^5 *N. sp. 1* spores, or 1.25×10^4 *N. displodere* spores for 30 minutes. Spores were washed off and infection progressed at 15°C. For the muscle-GFP strain HC46 *ccIs4251[myo-3::GFP-NLS, myo-3::GFP-MITO] I; mIs11[myo-2::GFP] IV*³⁴, 1000 synchronized L1 larvae were infected in duplicate at 15°C with $5.0\text{--}20.0 \times 10^4$ spores of *N. displodere* on a 6 cm plate. A fraction of animals was fixed in 4% PFA diluted in PBS + 0.1% Tween-20 at 24 hpi for FISH to verify infection distributions. At 76 hpi (*N. parisii* and *N. sp. 1*) or 120 hpi (*N. displodere*), animals were fixed for FISH with or without DY96 (10 μ g/ml) staining to stain infection and spores. DY96 stains chitin, which is a component of the spore wall³⁵. *N. displodere* FISH was performed as previously described⁵. All analysis and imaging was conducted on a Zeiss LSM700 confocal microscope with a 40x oil-immersion objective. The numbers of GFP⁺ host cell nuclei abutted by pathogen in a 3D stack of confocal images were counted to quantify the number of host cells that infection had spread into by the time of sporulation.

Measuring microsporidia growth by qPCR

The N2 strain was infected at the L1 stage at a dosage following the parameters described above for single microsporidia cell infections. Animals were fixed at various times post-inoculation in Extracta (Quanta Biosciences) to isolate DNA for qPCR-based analysis of growth. Microsporidia copy number was quantified with iQ SYBR Green Supermix (Bio-Rad) on a CFX Connect Real-time PCR Detection System (Bio-Rad). We measured the relative abundance of *Nematocida* and *C. elegans* DNA in 30 ng of DNA with the following primer sets: Np_rDNAF1: aaaaggcaccaggttgattc, Np_rDNAR1: agctctctgacgttccttc, Ce_snb-F1: ccggataagaccatcttgacg, Ce_snb-R1: gacgactcatcaacctgagc. Microsporidia copy number was measured by normalizing to samples infected by single microsporidia cells at early stages of growth when only a single nucleus is observed. We validated qPCR measurements of microsporidia copy number by taking a microscopy-based method of manually counting the average number of microsporidia nuclei per infection during growth from a single nucleus to 100 nuclei. Copy number measurement discrepancies between qPCR and manual count analyses were within 11%. Primer efficiencies were measured, and fold difference was calculated using the Livak comparative Ct method ($2^{-\Delta Ct}$).

Measuring animal size, egg number, and microsporidia spores

Animals were fixed and stained by FISH as described above, then imaged using a Zeiss AxioImager M1 upright fluorescent microscope with a 40X oil immersion objective. 50 animals per condition were manually outlined with Fiji software to calculate size (in μm^2). The number of eggs per animal was measured at 60 hpi by adding DY96 (4ng/ml with 0.1% SDS) to FISH-stained samples for 30 minutes before imaging. DY96 stains chitin, which is a component of the eggshell. The 60 hpi time point was chosen because it is when uninfected animals first consistently contain eggs. Eggs were counted in 50 animals per condition. Microsporidia spores also contain chitin, and were stained with DY96. Spore clusters per infected animal in 50 total animals per condition were counted. Each cluster of spores contained approximately 50 spores. Spore clusters (which we define as regions within meronts that contain approximately 30 spores with bright chitin staining) were counted at 52 hpi, which is the time at which single microsporidia cell infections begin to differentiate in to spores in N2 animals as described above.

Supplementary Material

Refer to Web version on PubMed Central for supplementary material.

Acknowledgments

We thank Michael Botts, Kirthi Reddy, and Aaron Reinke for helpful comments on the manuscript. Some *C. elegans* strains were provided by the Caenorhabditis Genetics Center, which is funded by National Institutes of Health (NIH) Office of Research Infrastructure Programs Grant P40 OD010440. This work was supported by National Science Foundation Graduate Research fellowships to KMB and to RJL, NIH grant R01GM114139, the David and Lucile Packard Foundation, and a Burroughs Wellcome Fund fellowship to ERT.

References

1. Gog JR, et al. Seven challenges in modeling pathogen dynamics within-host and across scales. *Epidemics*. 2015; 10:45–48. [PubMed: 25843382]

2. Casadevall A. Evolution of intracellular pathogens. *Annu Rev Microbiol.* 2008; 62:19–33. [PubMed: 18785836]
3. Troemel ER, Felix MA, Whiteman NK, Barriere A, Ausubel FM. Microsporidia are natural intracellular parasites of the nematode *Caenorhabditis elegans*. *PLoS Biol.* 2008; 6:2736–2752. [PubMed: 19071962]
4. Cuomo CA, et al. Microsporidian genome analysis reveals evolutionary strategies for obligate intracellular growth. *Genome research.* 2012; 22:2478–2488. [PubMed: 22813931]
5. Luallen RJ, et al. Discovery of a Natural Microsporidian Pathogen with a Broad Tissue Tropism in *Caenorhabditis elegans*. *PLoS Pathog.* 2016; 12:e1005724. [PubMed: 27362540]
6. Welch MD, Way M. Arp2/3-mediated actin-based motility: a tail of pathogen abuse. *Cell Host Microbe.* 2013; 14:242–255. [PubMed: 24034611]
7. Ciecionska M, Duncan R. Reovirus FAST proteins: virus-encoded cellular fusogens. *Trends Microbiol.* 2014; 22:715–724. [PubMed: 25245455]
8. French CT, et al. Dissection of the *Burkholderia* intracellular life cycle using a photothermal nanoblade. *Proc Natl Acad Sci U S A.* 2011; 108:12095–12100. [PubMed: 21730143]
9. Nikitas G, et al. Transcytosis of *Listeria monocytogenes* across the intestinal barrier upon specific targeting of goblet cell accessible E-cadherin. *J Exp Med.* 2011; 208:2263–2277. [PubMed: 21967767]
10. Swann J, Jamshidi N, Lewis NE, Winzeler EA. Systems analysis of host-parasite interactions. *Wiley Interdiscip Rev Syst Biol Med.* 2015; 7:381–400. [PubMed: 26306749]
11. Stentiford GD, et al. Microsporidia - Emergent Pathogens in the Global Food Chain. *Trends Parasitol.* 2016; 32:336–348. [PubMed: 26796229]
12. Cali, A.; Takvorian, PM. Microsporidia. John Wiley & Sons, Inc; 2014. Developmental Morphology and Life Cycles of the Microsporidia; p. 71-133.
13. Felix MA, Duveau F. Population dynamics and habitat sharing of natural populations of *Caenorhabditis elegans* and *C. briggsae*. *BMC biology.* 2012; 10:59. [PubMed: 22731941]
14. Bakowski MA, et al. Ubiquitin-mediated response to microsporidia and virus infection in *C. elegans*. *PLoS Pathog.* 2014; 10:e1004200. [PubMed: 24945527]
15. Balla KM, Troemel ER. *Caenorhabditis elegans* as a model for intracellular pathogen infection. *Cell Microbiol.* 2013
16. Legouis R, et al. LET-413 is a basolateral protein required for the assembly of adherens junctions in *Caenorhabditis elegans*. *Nat Cell Biol.* 2000; 2:415–422. [PubMed: 10878806]
17. Sapir A, Avinoam O, Podbilewicz B, Chernomordik LV. Viral and developmental cell fusion mechanisms: conservation and divergence. *Dev Cell.* 2008; 14:11–21. [PubMed: 18194649]
18. Altun ZF, HDH. Muscle system. *WormAtlas.* 2009
19. Altun ZF, HDH. Epithelial system. *WormAtlas.* 2009
20. Krishna S, Maduzia LL, Padgett RW. Specificity of TGFbeta signaling is conferred by distinct type I receptors and their associated SMAD proteins in *Caenorhabditis elegans*. *Development.* 1999; 126:251–260. [PubMed: 9847239]
21. Maduzia LL, et al. Ion-1 regulates *Caenorhabditis elegans* body size downstream of the dbl-1 TGF beta signaling pathway. *Dev Biol.* 2002; 246:418–428. [PubMed: 12051826]
22. Estes KA, Szumowski SC, Troemel ER. Non-lytic, actin-based exit of intracellular parasites from *C. elegans* intestinal cells. *PLoS Pathog.* 2011; 7:e1002227. [PubMed: 21949650]
23. Szumowski SC, Botts MR, Popovich JJ, Smelkinson MG, Troemel ER. The small GTPase RAB-11 directs polarized exocytosis of the intracellular pathogen *N. parisii* for fecal-oral transmission from *C. elegans*. *Proc Natl Acad Sci U S A.* 2014; 22:8215–8220.
24. Leitch GJ, Shaw AP, Colden-Stanfield M, Scanlon M, Visvesvara GS. Multinucleate host cells induced by *Vittaforma corneae* (Microsporidia). *Folia Parasitol (Praha).* 2005; 52:103–110. [PubMed: 16004369]
25. Morris DJ, Terry RS, Adams A. Development and molecular characterisation of the microsporidian *Schroederia airthreyi* n. sp. in a freshwater bryozoan *Plumatella* sp. (Bryozoa: Phylactolaemata). *J Eukaryot Microbiol.* 2005; 52:31–37. [PubMed: 15702977]

26. Stentiford GD, et al. *Areospora rohanae* n.gen. n.sp. (Microsporidia; Areosporiidae n. fam.) elicits multi-nucleate giant-cell formation in southern king crab (*Lithodes santolla*). *J Invertebr Pathol.* 2014; 118:1–11. [PubMed: 24566191]
27. Lom J, Dykova I. Microsporidian xenomas in fish seen in wider perspective. *Folia Parasitol (Praha)*. 2005; 52:69–81. [PubMed: 16004366]
28. Sprague GF Jr, Winans SC. Eukaryotes learn how to count: quorum sensing by yeast. *Genes Dev.* 2006; 20:1045–1049. [PubMed: 16651650]
29. Olive AJ, Sassetti CM. Metabolic crosstalk between host and pathogen: sensing, adapting and competing. *Nat Rev Microbiol.* 2016; 14:221–234. [PubMed: 26949049]
30. Brenner S. The genetics of *Caenorhabditis elegans*. *Genetics.* 1974; 77:71–94. [PubMed: 4366476]
31. Stiernagle, T. T.C.e.R. Community. *WormBook*. WormBook; 2006. Maintenance of *C. elegans*.
32. Gurskaya NG, et al. Engineering of a monomeric green-to-red photoactivatable fluorescent protein induced by blue light. *Nat Biotechnol.* 2006; 24:461–465. [PubMed: 16550175]
33. Schindelin J, et al. Fiji: an open-source platform for biological-image analysis. *Nat Methods.* 2012; 9:676–682. [PubMed: 22743772]
34. Winston WM, Molodowitch C, Hunter CP. Systemic RNAi in *C. elegans* requires the putative transmembrane protein SID-1. *Science.* 2002; 295:2456–2459. [PubMed: 11834782]
35. Hoch HC, Galvani CD, Szarowski DH, Turner JN. Two new fluorescent dyes applicable for visualization of fungal cell walls. *Mycologia.* 2005; 97:580–588. [PubMed: 16392246]

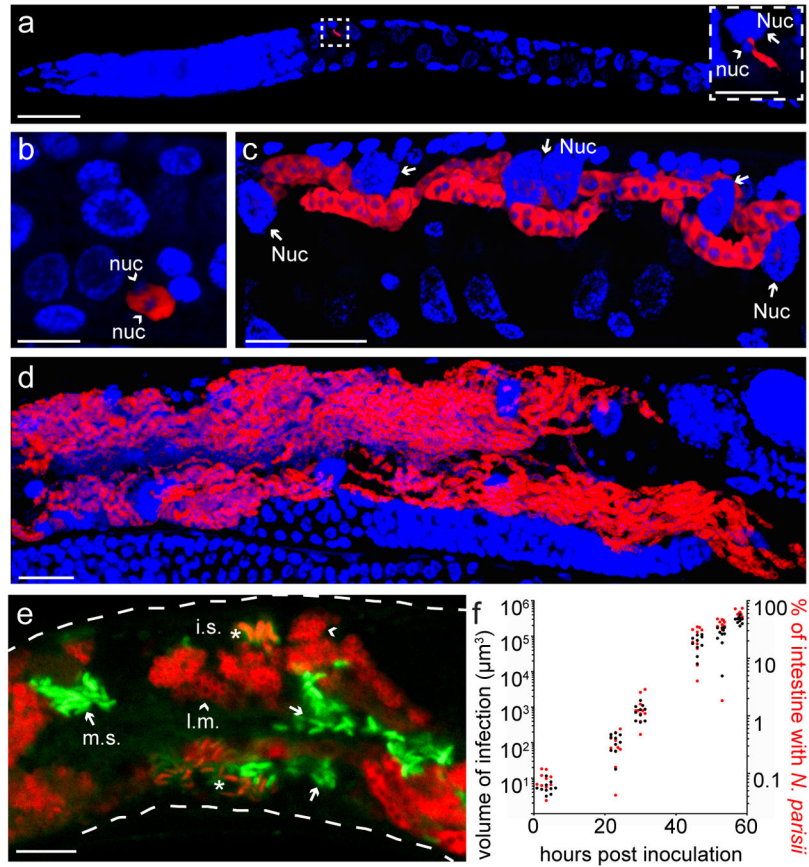


Figure 1. A single *N. parisii* cell can grow to fill most of the *C. elegans* intestine
 (a–d) Animals infected by a single *N. parisii* cell, then fixed and stained for DNA with DAPI (blue) and for *N. parisii* with an rRNA FISH probe (red). Images are 3D renderings of confocal z-stacks, and all images are oriented with the anterior of the animal to the left. (a) An animal infected by a single microsporidia cell 3 hpi. Scale bar spans 20 μm. The dashed box encloses a magnified region containing the microsporidia cell and its single nucleus (arrowhead, nuc) next to a larger host nucleus (arrow, Nuc). Scale bar within the box spans 5 μm. (b) Image of infection 18 hpi, marking the beginning of replication by the presence of two pathogen nuclei (arrowheads, nuc). Scale bar spans 5 μm. (c) Image of infection 36 hpi, in which the pathogen has replicated and grown across several intestinal cells (host nuclei indicated by arrows, Nuc). Scale bar spans 20 μm. (d) Image of infection 54 hpi, with extensive growth throughout the intestine and marking the beginning of sporulation. Scale bar spans 20 μm. (e) Magnified image of sporulation 54 hpi in an animal stained with an *N. parisii* rRNA FISH probe (red) and DY96 to label chitin (green). Microsporidia meronts begin to form rounded structures enclosing single nuclei (late meronts indicated by arrowheads, l.m.), rod-shaped cells bearing chitin (immature spores indicated by asterisks, i.s.), and fully formed spores that exclude FISH staining (mature spores indicated by arrows, m.s.). The dashed white line outlines the animal. Scale bar spans 10 μm. (f) Quantification of microsporidia growth from single cells over time in 10 individual animals. Each dot represents measurement of a single animal. Black dots correspond to measurements of

microsporidia volume (left y-axis), and red dots correspond to those same measurements expressed as a fraction of the total intestinal volume (right y-axis).

Author Manuscript

Author Manuscript

Author Manuscript

Author Manuscript

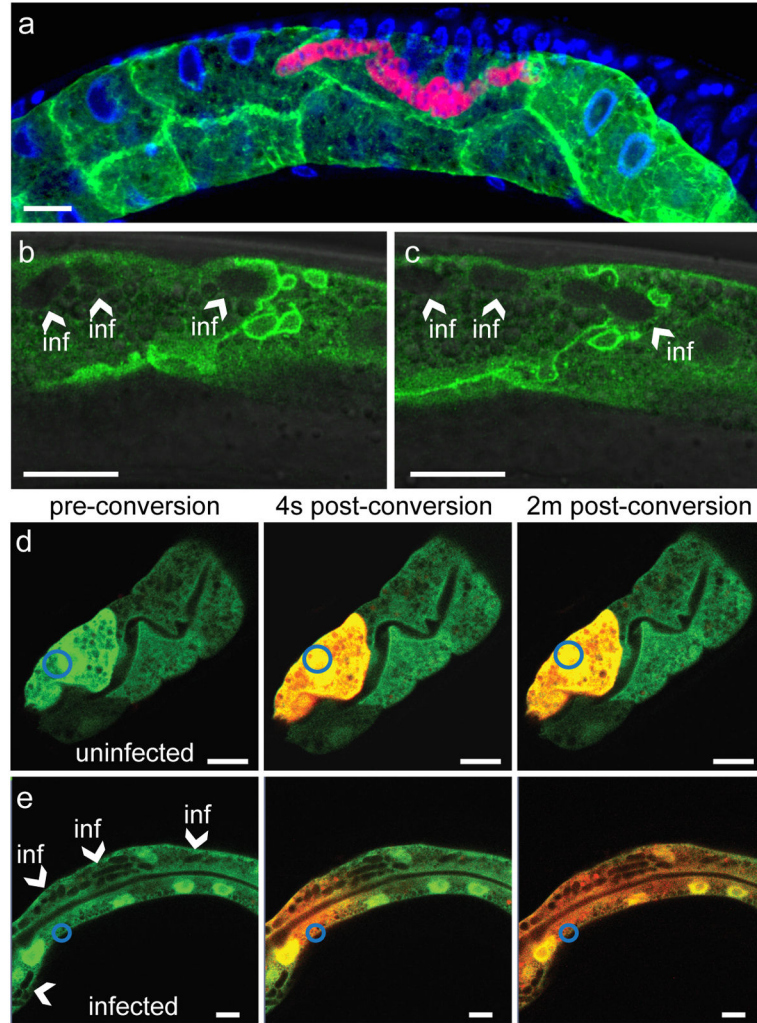


Figure 2. *N. parisii* can spread across and fuse host intestinal cells into a syncytial organ (a) Image of infection 31 hpi in a fixed transgenic animal expressing a GFP-labeled basolateral protein LET-413 in the intestine (green), stained for DNA with DAPI (blue) and *N. parisii* rRNA with FISH (red). (b) Image of a live infected GFP::LET-413 animal. *N. parisii* is unlabeled but observable as oval-shaped clearings in fluorescent signal (arrowheads). (c) Image of the same animal as in (b) but captured 1 minute later. (d–e) Images of a live uninfected (d) or infected (e) transgenic animal expressing the photoconvertible Dendra protein under an intestinal-specific promoter before conversion (left panel), four seconds after conversion (middle panel), and two minutes after conversion (right panel). Blue circle indicates the region that was targeted for photoconversion. Arrowheads in (e) point to areas in which *N. parisii* can be seen based on the absence of fluorescent signal. Scale bars in all images span 10 μm .

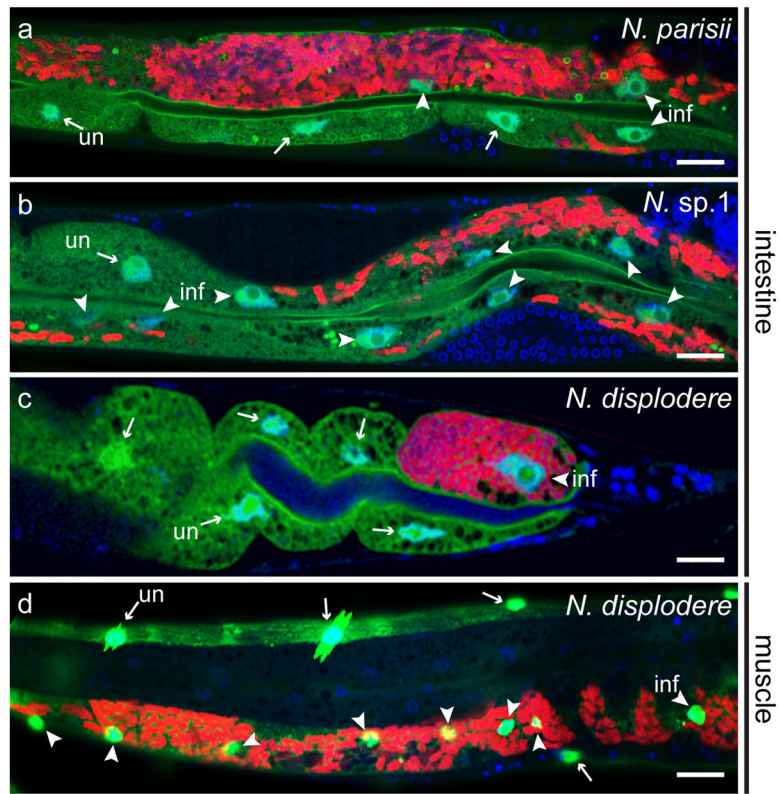


Figure 3. Spreading across host cells is a conserved microsporidia growth strategy with distinct host cell fusion patterns caused by distantly related *Nematocida* species

Images of single-cell infections by *N. parisii* (a), *N. sp. 1* (b), or *N. displodere* (c) in the intestine at the time of sporulation. Beginning of spore formation was 76 hpi for *N. parisii* and *N. sp. 1*, or 120 hpi for *N. displodere*, all at 15°C. Transgenic animals with GFP expressed in the cytoplasm and nuclei of intestinal cells (green) were fixed and stained for DNA with DAPI (blue) and *Nematocida* rRNA with FISH (red). Arrowheads point to host nuclei of cells with infection (inf), arrows point to host nuclei of cells without infection (un). Scale bars in all images span 20 μm. (d) Image of a single-cell infection by *N. displodere* in a transgenic animal with GFP expressed in the cytoplasm and nuclei of muscle cells. The green lines angled through two of the uninfected nuclei are artifacts from pixel saturation during image acquisition.

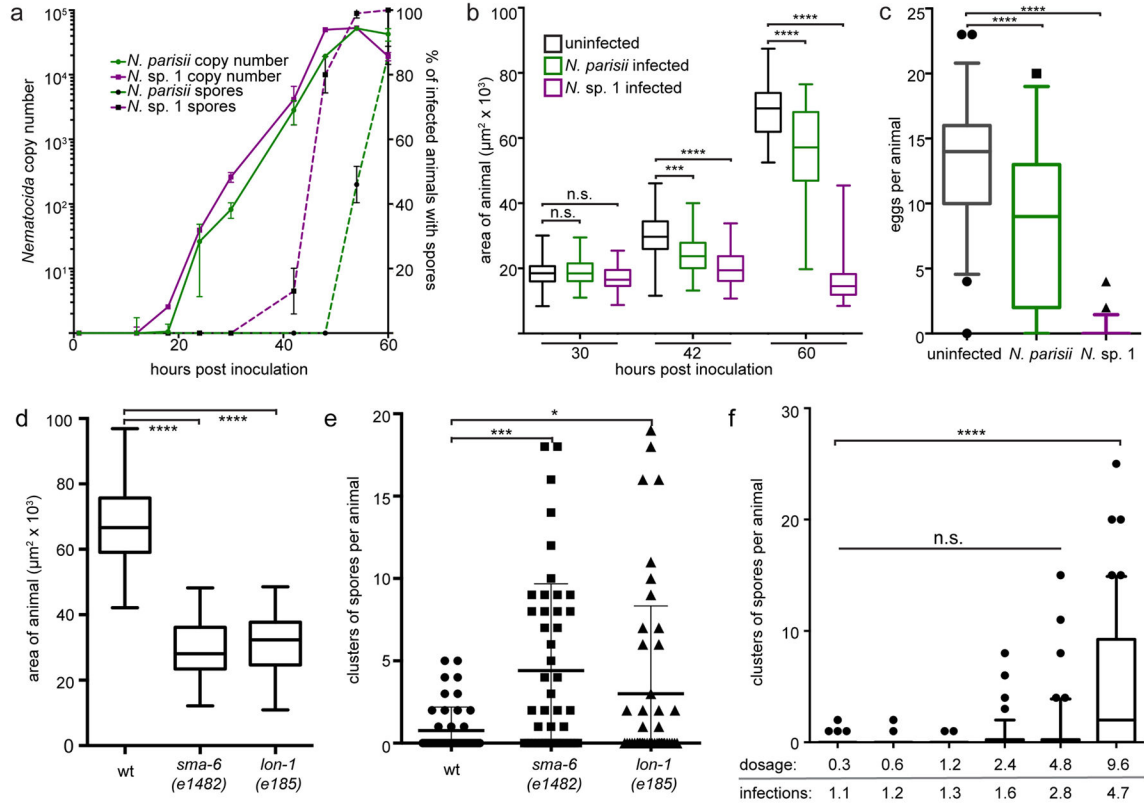


Figure 4. *Nematocida* vary in growth and virulence, and the density of infection alters developmental speed

(a) Growth kinetics of single-cell *N. parisii* and *N. sp. 1* infections. Purple lines correspond to *N. sp. 1* kinetics, green lines correspond to *N. parisii* kinetics. Solid lines show the kinetics of microsporidia copy number over time measured by qPCR with DNA extracted from 2000 animals, 40% of which were infected. Dashed lines show the kinetics of spore formation in the same populations of animals. Averages of two biological replicates are shown with standard deviation. (b) Sizes of animals infected by single *N. parisii* cells (green boxes) or *N. sp. 1* cells (purple boxes) compared to uninfected animals (black boxes) over time. Box-and-whisker plots include data from 50 animals per condition. (c) Eggs in 50 animals infected by single *N. parisii* cells (green boxes) or *N. sp. 1* cells (purple boxes) compared to uninfected animals (black boxes) at 60 hpi. (d) Sizes of wild-type and size mutant animals infected by single *N. parisii* cells 53 hpi. Box-and-whisker plots include data from 50 animals per condition. (e) Spore clusters per animal measured in the same animals as in (d). Dots represent measurements of individual animals; bars show averages with standard deviations. (f) Spore clusters per animal 52 hpi in populations that were pulse-infected with different dosages of *N. parisii* spores. Dosages of spores ($\times 10^6$) are shown underneath the graph, along with the average number of infections per animal at each dosage. Box-and-whisker plots include 95% of the data from measurements of 50 animals per condition; dots represent the remaining 5%. Significance was tested by one-way ANOVA, p-values generated with Tukey's multiple comparisons test and indicated by asterisks with *** 0.001, and **** 0.0001.